## III. Numerical and Experimental Results

Using (1)–(10), of present paper and [7, eqs. (28)–(31)], the VSWR and shunt admittance seen by the rectangular waveguide are evaluated for a coupling slot of length $2L = 1.7$ cm and width $2W = 0.107$ cm milled in a metal plate of thickness $t = 0.09144$ cm. The rectangular waveguide has dimensions $A = 1.016$ cm and $B = 2.286$ cm; the circular waveguide has radius $a = 1.185$ cm; and the frequency range is 8.2 to 9.4 GHz. The integrals appearing in [7, eqs. (30) and (31)] have been evaluated numerically using Gaussian quadrature [9], and the computations are carried out for different values of $N$.

The theoretical results on the variation of VSWR with frequency are presented in Fig. 3, together with the experimental results obtained from the measurement of return loss using an HP-8410C network analyzer and an HP-8747A waveguide reflection/transmission test set. The variations of normalized conductance and susceptance with frequency are presented in Fig. 4.

Computations are carried out for slot lengths ranging from 1.5 to 2.0 cm, for slot widths up to 0.6 cm, and for plate thicknesses up to 0.5 cm to study the effect of slot parameter variation on VSWR.

## IV. Discussion

A very good agreement between the theoretical and experimental results on the variation of VSWR with frequency justifies the validity of the theoretical formulations presented above. However, the minimum VSWR obtained (2.26) for slot dimensions of $2L = 1.7$ cm, $2W = 0.107$ cm, and $t = 0.09144$ cm is not satisfactory.

By changing the parameters of the junctions, it has been possible to reduce the minimum VSWR. From the numerical results, it is found that VSWR is favorably low for a slot width of 0.6 cm and a slot length of 1.6 cm. As the plate thickness is varied from zero to 0.35 cm, the minimum VSWR is reduced from 2.104 to 1.847 at a frequency of 9.6 GHz. When $t$ is increased to 0.5 cm, the minimum VSWR is found to be 1.741 at 9.6 GHz. The corresponding minimum insertion loss resulting from mismatch is about 2 dB. These minimum values are realized at the edge of the frequency band of interest. The VSWR and insertion loss are higher for other parameters. Since further reduction of VSWR and insertion loss using rectangular coupling slots is not possible in the frequency range of interest, it is suggested that the use of round ended slots may result in an improvement in the minimum VSWR and give rise to a better matched transition.

## References


[1] C. D. Montgomery, R. H. Dickie and E. M. Purcell, Eds., *Principles of Microwave Circuits* (MIT Radiation Laboratory Series, vol. 8). New York: McGraw-Hill, 1948.

[2] D. M. Sazonov, A. N. Gridin, and B. A. Mishustin, *Microwave Circuits*. Moscow: Mir Publishers, 1982.

[3] G. L. Ragan, Ed., *Microwave Transmission Circuits*. New York: McGraw-Hill, 1948.

[4] N. Marcuvitz, *Waveguide Handbook*. New York: Dover, 1965.

[5] H. Oraizi and J. Perini, "A numerical method for the solution of the junction of cylindrical waveguides," *IEEE Trans. Microwave Theory Tech.*, vol. MTT-21, pp. 640–642, Oct. 1973.

[6] H. Auda and R. F. Harrington, "A moment solution for waveguide junction problems," *IEEE Trans. Microwave Theory Tech.*, vol. MTT-31, pp. 515–520, July 1983.

[7] B. N. Das, P. V. D. Somasekhar Rao, and A. Chakraborty, "Narrow wall axial slot coupled T-junction between rectangular and circular waveguides," *IEEE Trans. Microwave Theory Tech.*, vol. 37, pp. 1590–1596, Oct. 1989.

[8] R. F. Harrington, *Time-Harmonic Electromagnetic Fields*. New York: McGraw-Hill, 1961.

[9] B. Carnaham, H. A. Luther, and J. O. Wilkes, *Applied Numerical Methods*. New York: Wiley, 1969.


# LED-Induced Distributed Bragg Reflection Microwave Filter with Fiber-Optically Controlled Change of Center Frequency via Photoconductivity Gratings

Walter Platte

*Abstract*—**A light-induced distributed Bragg reflection band-reject microwave filter is reported in which the grating elements are optoelectronically generated through periodic-structure photoexcitation of a silicon coplanar waveguide. The center frequency can be optically adjusted to 11 GHz and 22 GHz, respectively, by means of a pattern-controlled fiber bundle array fed from six CW-operated 50 mW, 840 nm LED's. Experimental results are in good agreement with theoretical predictions. The principle of operation demonstrated also applies to millimeter-wave integrated circuits.**

## I. Introduction

It is known that the distributed Bragg reflection (DBR) characteristics of a periodic-structure waveguide or transmission line can successfully be utilized for the realization of frequency-selective microwave or millimeter-wave devices such as band-reject filters [1] and grating reflectors, e.g., in a stabilized-feedback Gunn oscillator [2], [3]. Usually, the periodic perturbation in the direction of wave propagation is achieved by abrupt changes in permittivity or cross-sectional dimensions (e.g., reduced waveguide thickness [1]–[3]), thus producing a permanent, normally noncontrollable grating structure.

However, when replacing the total dielectric (or a suitable cross-sectional portion of it) by semiconductor material, it is possible to generate the grating configuration optoelectronically [4]–[6]. For this purpose, the originally homogeneous, unperturbed semiconductor waveguide or transmission line is photoexcited by a locally varying periodic illumination, e.g. by means of a pattern-controlled LED-fed fiber bundle array of the type shown in Fig. 1, which correspondingly causes a periodic distribution of the photoinduced charge carriers inside the semiconductor material. Thus, a nonpermanent photoconductivity grating is created, exhibiting the well-known stopband phenomenon [7] within the nonradiating region of the structure. Since the lengths $l_1$ and $l_2$ of the excited and dark sections (Fig. 1(b), (c)), the period $\Lambda$, the total length of the grating structure, and the amount of photoconductivity (forming the "depth" of the grooves) can be changed by altering the illumination pattern and the intensity, the filter parameters (i.e., center frequency, bandwidth, and reflectance) can be fiber-optically controlled. The price one pays for this capability, however, manifests itself in the optically induced losses which clearly injure the reflection and selectivity characteristics. Moreover, the microwave or millimeter-wave performance of an optically CW-generated DBR structure is governed by the inherent carrier diffusion mechanisms in such a way that the transverse diffusion mainly influences the light-induced losses [8], whereas the longitudinal car-

Manuscript received March 21, 1990; revised July 31, 1990.

The author is with the Institut fuer Hochfrequenztechnik, Universitaet Erlangen–Nuernberg, D-8520 Erlangen, Germany.

IEEE Log Number 9041081.

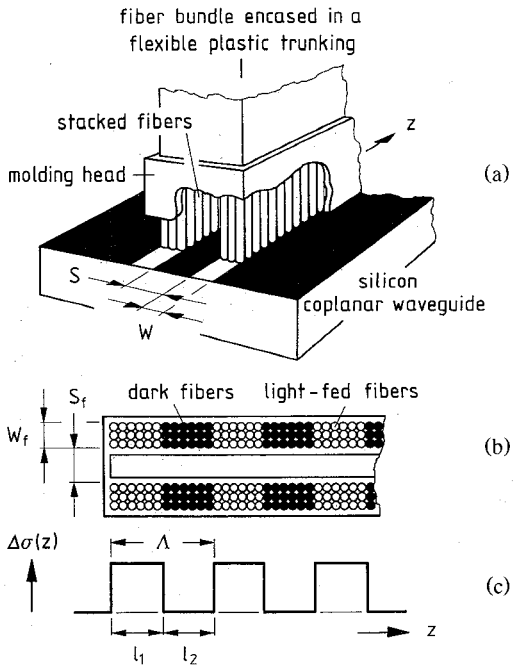


Fig. 1. Sketch of light-induced DBR microwave filter on silicon substrate illuminated by a pattern-controlled LED-fed fiber bundle array on top of the coplanar waveguide. (a) Total configuration with cutaway section of the molding head. (b) Cross-sectional view of the molding head. (c) Longitudinal distribution of photoconductivity $\Delta\sigma(z)$ forming the grating profile.

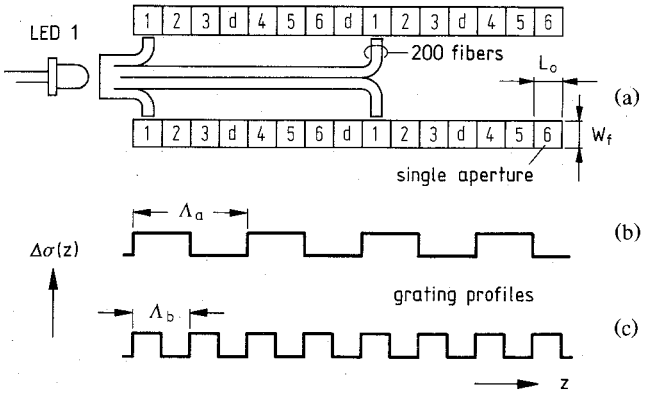


Fig. 2. (a) Specific fiber-feeding scheme exhibiting the array-internal transfer of light and the assignment of the 30 individual apertures to the six LED's numbered 1 through 6, $d$ indicates permanently dark apertures. (b) Photoconductivity profile $\Delta\sigma(z)$ with LED's 1, 2, 4, and 5 activated ($f_c = 11$ GHz, $n = 0$, $N = 4$). (c) Profile with LED's 1, 3, 4, and 6 activated ($f_c = 22$ GHz, $n = 0$, $N = 8$.)

rier diffusion (in the direction of wave propagation) effects a smooth broadening of the grating profile, which reduces reflectance and selectivity [6], [9].

The band-reject filter reported here is based on the quasi-TEM-mode wave propagation in a silicon coplanar waveguide (Si CPW) [10]. In comparison with the plasma-induced TE-mode DBR structure in a closed-type semiconductor waveguide [4], this planar transmission line version offers the advantage of being operated by low-power light sources without the need for any heat sinking. Moreover, the Si CPW configuration is compatible with MIC devices and techniques, and the controlling optical power can easily be supplied to the open semiconductor surface.

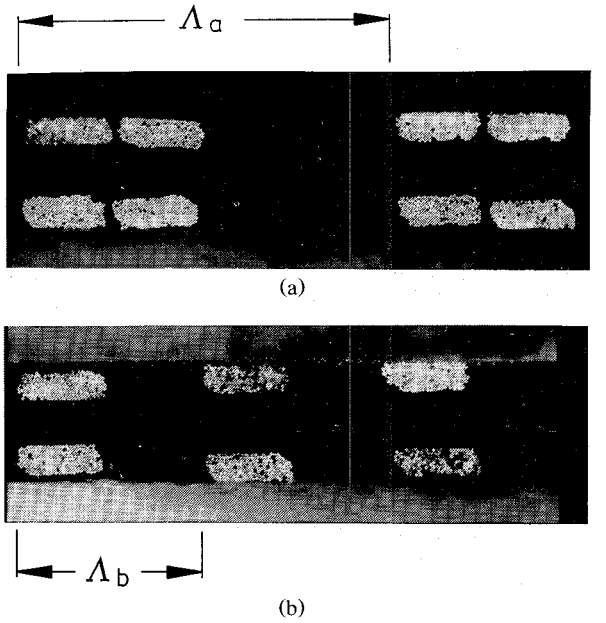


Fig. 3. Partial photograph of the fiber bundle array used, just generating a symmetric ($n = 0$) twin-stripe illumination pattern for (a) $f_c = 11$ GHz with $\Lambda_a = 5.40$ mm and (b) $f_c = 22$ GHz with $\Lambda_b = 2.70$ mm.

This paper reports the first laboratory specimen of an LED-induced pattern-controlled DBR filter structure for demonstrating both the principle and the feasibility of a fiber-optical changeover of center frequency.

## II. Filter Characterization from Abrupt-Profile Approach

Referring to, on the one hand, the specific fiber-feeding scheme (Fig. 2) and the resultant illumination pattern (Fig. 3) and, on the other, the substrate parameters presented in Section III, it is seen that, for both values of operating center frequency, the suitably adjusted length $l_1$ of the excited grating section is much greater than the ambipolar diffusion length $L_a$ of the optically generated charge carriers. In this case, the diffusion-controlled broadening of the photoinduced grating profile [6] can be neglected; hence, the filter structure actually works under the abrupt-profile excitation condition. This allows the grating reflection coefficient $\Gamma_{n,N}$ to be approximately calculated from the following expression [5]:

$$\Gamma_{n,N} \simeq \frac{(1-j\Delta\vartheta_e)^{-0.5}-1}{(1-j\Delta\vartheta_e)^{-0.5}+1}\left\{1-\exp\left[-2l_1(\alpha_0+\Delta\alpha+j\beta_l)\right]\right\} \times \sum_{\nu=1}^{N} \exp\left\{-2(\nu-1)\left[(\alpha_0+j\beta_l)(l_1+l_2)+\Delta\alpha l_1\right]\right\} \quad (1)$$

where $n$ is the illumination pattern coefficient, and $N$ is the number of grating elements. $\alpha_0$ is the attenuation constant of the dark Si CPW which, in the present case, is additionally loaded with the fiber array dielectrics; $\Delta\alpha$ indicates the contribution of attenuation from light-induced losses [8], and $\beta_l$ is the phase constant of a lossless (but equally loaded) CPW [6]. $\Delta\vartheta_e$ is the effective photoconductivity loss tangent according to $\Delta\vartheta_e = 2\Delta\alpha/\beta_l$, where $\Delta\vartheta_e \lesssim 1$ has been assumed for the abrupt-profile analysis [5], this requiring low photoexcitation and/or sufficiently high frequencies. Since this approach is based on the small-reflection theory, (1) holds true as long as $|\Gamma_{n,N}| \lesssim 0.40$ [6].

When assuming $N \gg 1$, the specific grating dimensions $l_1$ and $l_2$ (Fig. 1(b), (c)) are approximately given by

$$l_1 \simeq c_0/4(n+1)f_c\sqrt{\epsilon_{re}} \tag{2}$$

and

$$l_2 = (2n+1)l_1 \qquad \text{with } n = 0,1,2,\cdots \tag{3}$$

where $l_1 + l_2 = \Lambda$, $c_0$ is the velocity of light in free space, $f_c$ is the center frequency, and $\epsilon_{re}$ is the overall effective dielectric constant of the Si CPW, including the dielectrics of the fiber bundle molding head (Section III).

Now, the characterization of any light-induced Si CPW filter structure with arbitrary values of $f_c$, $n$, and $N$ can easily be accomplished by means of the excitation-dependent DBR spectrum $|\Gamma_{n,N}(f)|$ resulting from (1)–(3), provided that $\epsilon_{re}$, $\Delta\alpha$, and $\alpha_0$ are known. In practice, $\Delta\alpha$ and $\epsilon_{re}$ can be computed with sufficient accuracy [8], [10], whereas $\alpha_0$ should be determined by experiment, bearing in mind that the loss tangent of the compound-dielectric molding head used is largely unknown, especially at microwave and millimeter-wave frequencies.

Concerning the actual filter structure detailed in Section III, the following relations have been obtained: $\beta_l/\text{rad cm}^{-1} = 0.5314 \cdot f/\text{GHz}$ along with $\epsilon_{re} = 6.432$, $\Delta\alpha/\text{dB cm}^{-1} = 4.29 \times 10^{-3} \cdot p/\text{mW cm}^{-2}$, where $p$ is the controlling irradiance, and $\alpha_0/\text{dB cm}^{-1} = 6 \times 10^{-3} \cdot f/\text{GHz} + 1.3 \times 10^{-3} \cdot (f/\text{GHz})^2$ [11]. The resultant (theoretical) reflection spectra associated with the two specific excitation conditions stated below are presented in Fig. 5.

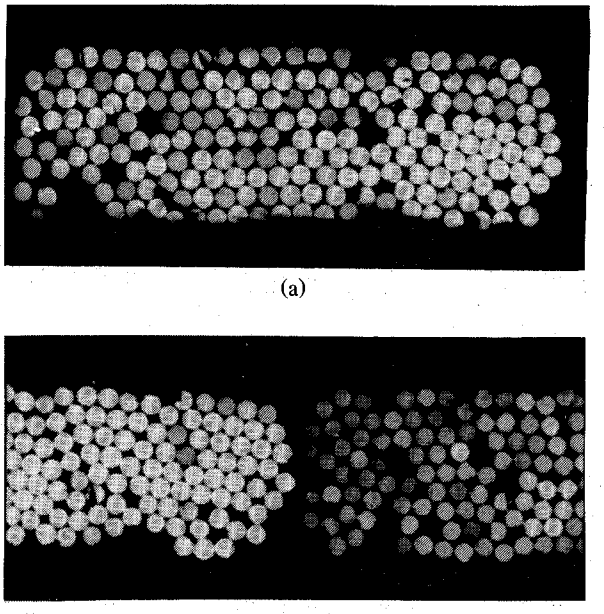

Fig. 4. Detailed illustrations of (a) actual fiber stacking and shape of aperture and (b) typical boundary between two adjoining apertures (which were differently activated for picture-taking purposes).

## III. Design of Silicon CPW and Fiber Bundle Array

The test CPW consists of a silicon substrate measuring 2.54 cm × 2.54 cm × 0.05 cm with a gold metallization of about 7 $\mu$m thickness. The substrate parameters are relative permittivity $\epsilon_r = 11.7$, dark conductivity $\sigma_d = 2.5 \times 10^{-4}$ $(\Omega\ \text{cm})^{-1}$, carrier mobility $(\mu_n + \mu_p) = 2100\ \text{cm}^2/\text{Vs}$, carrier lifetime $\tau = 1\ \mu\text{s}$, ambipolar diffusion length $L_a = 47\ \mu$m, surface recombination velocity $v_s = 2 \times 10^3$ cm/s, surface reflectivity $R = 0.30$, and peak photosensitivity wavelength $\lambda_p = 860$ nm, all quoted from the manufacturer's specification sheet.

The fiber bundle array is positioned in such a way that its light-emitting stacked-fiber region touches the surface of the CPW. Although actually composed of various materials of finite extent (with Plexiglas housing $\epsilon_r = 2.59$, fiber $\epsilon_r = 3.78$, and epoxy resin $\epsilon_r = 3.78$), the molding head is assumed to fill the total half-space above the CPW, taking account of an equivalent mixed-dielectric head permittivity of $\epsilon_{rh} = 3.30$ [11]. Since the effects of upper half-space dielectric loading and substrate photoexcitation can easily be studied (and incorporated into the dimensional design of Si CPW) by means of an equivalent CPW configuration of infinite substrate thickness and zero metallization thickness, this method is utilized here for the calculation of characteristic impedance $Z_l$ [10] and optically induced attenuation constant [8]. Following this concept, the given substrate permittivity is changed into an equivalent (infinite-substrate) value, namely $\epsilon_{rs} = 9.564$ in the present case [11]. From this, $\epsilon_{re} = 6.432$ has been obtained according to $\epsilon_{re} = (\epsilon_{rs} + \epsilon_{rh})/2$, which finally yields both the effective and the actual aspect ratio $k_e = 0.4559$ and $k = 0.4356$, respectively, for $Z_l = 50\ \Omega$ [10], where $k = S/(S+2W)$ with strip width $S$ and slot width $W$ (Fig. 1(a)). Referring to the conductor dimensions of the CPW-to-coaxial adapters used (SMA) and taking account of the intent to ensure the required uniform photoexcitation of the groove sections through multiple-fiber illumination, $S = 710\ \mu$m along with $W = 460\ \mu$m has been considered most suitable.

Further, substituting the radiation absorption coefficient $\alpha_r = 700\ \text{cm}^{-1}$ associated with 840 nm excitation of silicon, the theory of photoinduced losses in Si CPW [8] yields an effective photoconductivity $\Delta\sigma_e/(\Omega\text{cm})^{-1} = 10^{-4} \cdot p/\text{mW cm}^{-2}$, effective and normalized plasma penetration depths $d_e = 66\ \mu$m and $\delta = 0.186$, respectively [12], and a plasma filling fraction $q_p = 0.130$, where $q_p$ is identical to the term $s/K$ used in [8]. Finally, by incorporating the dielectric (semiconductor) filling fraction $q_\epsilon = 0.50$, one obtains $\Delta\alpha$ as mentioned in Section II.

The controlling radiation is guided through a shape-changing fiber bundle configuration which comprises six subbundles, each coupled to a 50 mW LED (Hitachi HLP 50 RC, $\lambda = 834 \cdots 854$ nm) via 800 individual step-index fibers used in parallel. At their output ends, the subbundles are split, stacked, and potted in an epoxy resin molding such that a twin-stripe multilayer fiber bundle array of stripe width $W_f = 470\ \mu$m, spacing $S_f = 700\ \mu$m, and 20.25 mm total length is created (Fig. 1(b)). Owing to $W < W_f$ and $S > S_f$, the light-emitting area slightly overlaps the CPW slot region for the purpose of easier molding head adjustment. Differing from the arrangement sketched in Fig. 1, the stripe spacing has been realized by a Plexiglas filling to achieve better stability and homogeneity of the dielectric loading.

The array-internal assignment of the individual fibers to the six LED's has been accomplished in accordance with the specific fiber-feeding scheme illustrated in Fig. 2. According to the actual array configuration, where 15 equal-sized stacked-fiber regions (Fig. 4(a)) have been lined up to form a stripe, the sketched arrangement exhibits 2 × 15 areas, each labeled with a numeral from 1 through 6 which indicates the feeding LED. For instance, the light transfer from LED 1 to the corresponding apertures is illustrated in Fig. 2 as well. Areas marked with a $d$ represent those regions which normally remain dark, but, nevertheless, contain a stacked-fiber filling to avoid (permanent) periodic modulation of permittivity within the molding head. Since both stripes are equally composed and fed, the Si CPW is operated under symmetric twin-slot excitation.

The length $L_0$ of the light-emitting apertures has been chosen as 1.35 mm so as to give center frequencies of about 11 GHz and 22 GHz, respectively. Hence, for example, an 11 GHz excitation profile of period $\Lambda_a$ can be obtained with LED's 1, 2, 4, and 5 in the ON state ($N = 4$, $n = 0$, $l_1 = l_2 = 2L_0$, Fig. 2(b)),

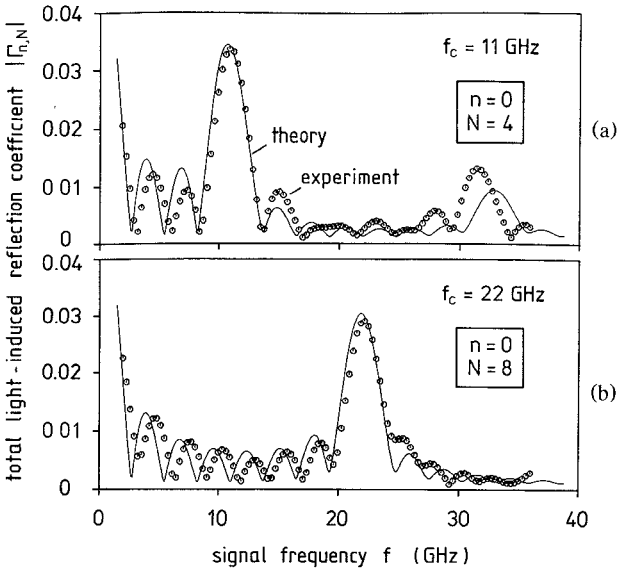


Fig. 5. Measured and calculated reflection spectra: (a) $|\Gamma_{0,4}(f)|$ with $f_c = 11$ GHz and (b) $|\Gamma_{0,8}(f)|$ with $f_c = 22$ GHz. The incident CW irradiance was $p = 110$ mW/cm$^2$.

whereas a 22 GHz excitation profile of period $\Lambda_b$ results from LED's 1, 3, 4, and 6 powered ($N = 8$, $n = 0$, $l_1 = l_2 = L_0$, Fig. 2(c)). Further, the device is capable of generating another 11 GHz grating with LED's 2, 3, 5, and 6 powered, thereby exhibiting a DBR characteristic with phase quadrature relative to the 1–2–4–5-excited one. Also, 11 GHz gratings ($N = 4$, $n = 1$) with 0°, 90°, or 180° DBR phase shift can be induced by activating LED's 1+4, 2+5, or 3+6. Thus, fiber-optically controlled phase shift keying is possible.

Fig. 3 shows a partial photograph of the fiber bundle array realized, just generating a symmetric twin-stripe illumination pattern for (a) 11 GHz and (b) 22 GHz. Fig. 4 illustrates in detail the actual fiber stacking and the shape of (a) one of the apertures comprising 200 individual fibers nominally, as well as (b) the boundary between two (differently activated) adjoining apertures. In place, the homogeneity of light emission is injured, obviously due to fiber breakage.

## IV. Results and Discussion

Measurements of the light-induced 11 GHz and 22 GHz DBR spectra were performed by means of an automatic vector network analyzer (Wiltron 360+3621 A, 0.04–40 GHz) operated in the gating mode, thereby eliminating the effects of imperfect adapters. In the other cases the experimental results were obtained from a vector subtraction procedure as described in [6]. As the actually usable length of the test CPW was only 20.25 mm, the fiber-optically controlled change of center frequency could only be carried out with $N = 4$ and $N = 8$, respectively. Thus, the experimental results reported here may only be considered a verification of the principle of operation. Owing to separate driver circuits, the currents through the LED's could individually be adjusted in order to produce a measured quasi-homogeneous irradiance of 110 mW/cm$^2$ [11].

As a result, Fig. 5 shows the measured reflection spectra $|\Gamma_{0,4}(f)|$ with $f_c = 11$ GHz (a) and $|\Gamma_{0,8}(f)|$ with $f_c = 22$ GHz (b). For comparison, the computed reflection spectra (Section II) in the case of perfectly matched termination [6] have been recorded in Fig. 5 as well. It is seen that, in practice, a slight shift of center frequency with respect to the nominal value occurs. This is presumed to arise from the fact that, although the condition $N \gg 1$ is not fulfilled here, the design of the fiber bundle array ($l_1, l_2, L_0$) has been based on (2) and (3); in addition, the theoretical $\epsilon_{re}$ value used can only approximately describe the actual CPW arrangement. Concerning the absolute magnitude of light-induced reflection coefficient, Fig. 5 obviously exhibits good agreement between theoretical and experimental results, thereby verifying the abrupt-profile DBR analysis [5] and, in particular, the theory of optically CW-induced losses in a semiconductor CPW [8].

## V. Concluding Remarks

In this paper, the design and experimental investigation of the first prototype of a fiber-optically controlled DBR Si CPW microwave filter have been reported. As the fabrication of the fiber bundle array was anticipated (and, indeed, has been confirmed) to be very complicated, the specific dimensions $W_f$ and $L_0$ of the light-emitting apertures have been chosen to be relatively large, so as to reduce the effects of stacking tolerances and misalignment of the individual apertures. Thus, a quasi-abrupt grating profile of piecewise-uniform photoconductivity was generated through multiple-fiber illumination. Of course, such a "large-area" photoexcitation (0.64 mm$^2$ area of aperture) was attended with low irradiance in this case, considering the optical power available, which resulted in very small stopband reflection coefficients not exceeding 4%. Much better efficiency (and better selectivity as well) could be attained from asymmetric excitation profiles ($n = 1, 2, \cdots$ [6], [13]) along with small-area apertures. This, however, would require more experience in the fabrication of pattern-controlled fiber bundle arrays.

Provided that a mature stacking technique is available, it should be possible to realize much smaller apertures with $L_0$ and $\Lambda$ ranging from 200 $\mu$m to 600 $\mu$m (along with correspondingly reduced CPW dimensions), thereby increasing the number of grating elements to $N = 20 \cdots 40$ across an acceptable total length of $10 \cdots 20$ mm. This, in conclusion, would considerably improve the DBR efficiency and selectivity [13], clearly without the need for higher optical power. Hence, the method of periodic-structure photoexcitation could be extended to the millimeter-wave range and, consequently, would open the interesting potential of novel millimeter-wave integrated circuit applications.

Moreover, it has been demonstrated from a numerical optimization of the reflection and selectivity characteristics with respect to $N$, $n$, and $p$ [13] that optimized LED-induced DBR filters are capable of producing a reflection–selectivity product RSP[1] of about $15 \cdots 25$ and thus are certainly comparable to dielectric permanent-grating structures. (See, for example, the inverted-strip dielectric waveguide band-reject filter [1] with $N = 30$ and $n = 1$ which exhibits 500 MHz bandwidth at 15.55 GHz center frequency along with 1.5 dB grating return loss, yielding RSP $\approx$ 26.)

Finally, a more futuristic idea is to operate the Si CPW under single-slot photoexcitation together with single-fiber illumination where the two array stripes are differently fed (each associated with different center frequencies for multiple changeover) and the light-emitting aperture per grating element has reduced to the core cross section of a single fiber. In this case, assuming sufficiently low carrier lifetimes, a symmetric-profile photoexcitation ($n = 0$) would result in a quasi-sinusoidal distribution of photoconductivity, which clearly implies a modification of the theory used so far. Corresponding investigations are currently in progress.

[1]RSP is the product of the maximum reflection coefficient at center frequency and the reciprocal of the relative bandwidth.

ACKNOWLEDGMENT

The author would like to thank B. Schmauss and M. Loeffler for performing the measurements, and the firm H. Hund GmbH, Wetzlar, Germany, for fabrication of the fiber bundle array.

REFERENCES

[1] T. Itoh, "Application of gratings in a dielectric waveguide for leaky-wave antennas and band-reject filters," *IEEE Trans. Microwave Theory Tech.*, vol. MTT-25, pp. 1134–1138, 1977.
[2] T. Itoh and F. J. Hsu, "Distributed Bragg reflector Gunn oscillators for dielectric millimeter-wave integrated circuits," *IEEE Trans. Microwave Theory Tech.*, vol. MTT-27, pp. 514–518, 1979.
[3] B. S. Song and T. Itoh, "Distributed Bragg reflection dielectric waveguide oscillators," *IEEE Trans. Microwave Theory Tech.*, vol. MTT-27, pp. 1019–1022, 1979.
[4] M. Matsumoto, M. Tsutsumi, and N. Kumagai, "Bragg reflection characteristics of millimeter waves in a periodically plasma-induced semiconductor waveguide." *IEEE Trans. Microwave Theory Tech.*, vol. MTT-34, pp. 406–411, 1986.
[5] W. Platte, "Optical control of microwaves by LED-induced DBR structures in silicon coplanar waveguides," *Electron. Lett.*, vol. 25, pp. 177–179, 1989.
[6] W. Platte, "Periodic-structure photoexcitation of a silicon coplanar waveguide for selective optoelectronic microwave control," *IEEE Trans. Microwave Theory Tech.*, vol. 38, pp. 638–646, May 1990.
[7] G. L. Matthaei, L. Young, and E. M. T. Jones, *Microwave Filters, Impedance-Matching Networks, and Coupling Structures*. New York: McGraw-Hill, 1964.
[8] W. Platte and B. Sauerer, "Optically CW-induced losses in semiconductor coplanar waveguides," *IEEE Trans. Microwave Theory Tech.*, vol. 37, pp. 139–149, 1989.
[9] W. Platte, "Influence of charge carrier diffusion on the microwave performance of fiber-optically generated DBR filter structures," *Arch. Elek. Übertragung.*, vol. 44, pp. 282–290, 1990 (in German).
[10] K. C. Gupta, R. Garg, and I. J. Bahl, *Microstrip Lines and Slotlines*. Norwood, MA: Artech House, 1979.
[11] M. Loeffler, B. Schmauss, and W. Platte, Internal Rep. IHFT-DA 541, Univ. Erlangen–Nuernberg, Erlangen, Germany, 1989.
[12] W. Platte, "Effective photoconductivity and plasma depth in optically quasi-CW controlled microwave switching devices," *Proc. Inst. Elec. Eng.*, pt. J., vol. 135, pp. 251–254, 1988.
[13] W. Platte, "Fiber-optically induced DBR microwave filter structures with optimized reflection and selectivity characteristics," *Arch. Elek. Übertragung.*, vol. 44, pp. 291–296, 1990 (in German).

# Determination of Intrinsic FET Parameters Using Circuit Partitioning Approach

Hans-Olof Vickes

*Abstract*—**A technique useful in extracting intrinsic parameters for a compound semiconductor FET is presented. The technique makes use of a method provided by Dambrine *et al.* [8]. A modified active circuit that accounts for charge accumulation in the conducting channel is presented. The model has the further advantage of using control voltage modeling in agreement with the Curtice convention for large-signal analysis. The equations are presented for each active element as a function of the intrinsic *y* parameters. Measurements verify the parameter extraction technique with the circuit topology used and show good results.**

Manuscript received August 23, 1989; revised July 31, 1990. This work was supported by the National Board for Technical Development (STU).

The author was with the Division of Network Theory, Chalmers University of Technology, S-412 96, Gothenburg, Sweden. He is now with the Aerospace Division, Ericsson Radar Electronics AB, R/ST S-43184 Mölndal, Sweden.

IEEE Log Number 9041090.

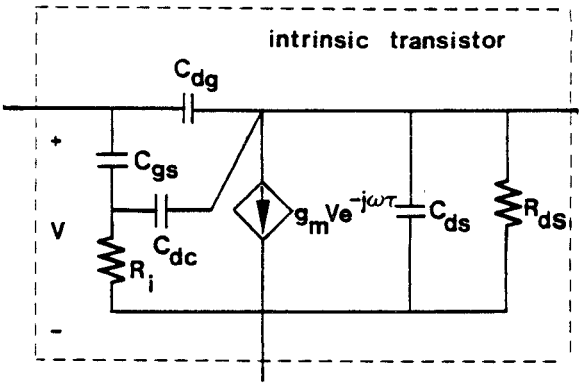


Fig. 1. Active FET model with control voltage modeled over the total $C_{gs}-R_i$ combination (after Curtice [10]). The current source is modeled with a linear transconductance, $g_m$, and an associated transit time delay, $\tau$.

## I. INTRODUCTION

A physically based small-signal equivalent circuit of a field-effect transistor is very useful in the development of new circuit design guidelines for both microwave and digital GaAs integrated circuits. Such a model is usually obtained by optimizing the component values to closely fit the small-signal microwave scattering parameters for the device in question. However, this circuit parameter determination technique is old-fashioned and is not advisable because it has several drawbacks:

i) The unduly large number of variables for the optimization algorithm (likelihood of stopping at a local minimum).
ii) Several resulting element values become dependent upon optimization.

Thus, using this technique we can obtain a physically invalid circuit [1].

To overcome these difficulties appropriate decomposition schemes should be considered. Important contributions with special relevance to microwave decomposition can be found in [2]–[8]. The method developed by Dambrine *et al.* [8] seems to be the most powerful measurement technique yet described.

The objective of this paper is to exploit the above method of extraction of the intrinsic *y* parameters for a better understanding of the high-frequency performance of compound semiconductor FET's. Thus, by using simple matrix manipulations, the intrinsic matrix is determined. Here we further develop and refine the intrinsic FET description. In addition, we use a symmetrical T network to model the coplanar waveguide with lower ground plane (CPWG) at the input and output terminals of the device in question. In this manner, we can show how an accurate FET equivalent circuit topology is used to generate high-frequency equivalent circuits for compound semiconductor FET's.

## II. ANALYSIS

The measurement technique of the extrinsic elements constitutes a key point in the paper by Dambrine *et al.* [8] and is clearly explained. Therefore, in this paper we focus on the intrinsic FET description. To examine the small-signal intrinsic *y* parameters of compound semiconductor FET's, we use the